

Extracting an accurate model for permittivity from experimental data : Hunting complex poles from the real line

M. GARCIA-VERGARA^{1,*}, G. DEMÉSY¹, AND F. ZOLLA¹

¹Aix Marseille Université, CNRS, Centrale Marseille, Institut Fresnel UMR 7249, 13013 Marseille, France

*Corresponding author: mauricio.garcia-vergara@fresnel.fr

Abstract

In this letter, we describe a very general procedure to obtain a causal fit of the permittivity of materials from experimental data with very few parameters. Unlike other closed forms proposed in the literature, the particularity of this approach lies in its independence towards the material or frequency range at stake. Many illustrative numerical examples are given and the accuracy of the fitting is compared to other expressions in the literature.

1 Introduction

In this letter, we propose a general framework dedicated to the fitting of tabulated experimental data of complex permittivities [1, 2]. When using time harmonic numerical methods in electromagnetism, one sets a real frequency and uses the tabulated data, up to a simple interpolation, as it is. However, in time domain methods (e.g. Finite difference [3], discontinuous Galerkin [4]), the inverse Fourier Transform of the experimental data is needed since frequency dispersion in the time domain is generally tackled through an extra differential equation involving the polarization vector. An analytical expression of the relative permittivity $\hat{\epsilon}_r(\omega)$ fulfilling causality requirements has to be extracted from the data given in frequency domain. Same considerations hold when tackling generalized modal computations [5] of dispersive structures. This problem is well known and several closed forms have already been proposed: Drude and/or Drude-Lorentz model, Debye model, critical points model [6], or a combination of these elementary resonances [7, 8]. It is worth noticing that the form assumed is material dependent in the literature. In this letter we do not assume any particular form for the permittivity. The only

requirement is the causality principle handled via the general constitutive relation between the electric field \mathbf{E} and the polarization vector \mathbf{P}_e . Causality is also ensured by assuming numerically that the experimental data satisfy appropriate parity requirements. We provide the details of the iterative least square approach, and provide numerical illustrations for semi-conductors and metals.

2 Mathematical formulation

In a frequency dispersive material with negligible magnetization, the electric displacement \mathbf{D} is not only influenced by the electric field \mathbf{E} , but also by the polarization vector \mathbf{P}_e . A very general approach is to consider the following constitutive relation:

$$\sum_{l=0}^{N_d} q_l \frac{\partial^l \mathbf{P}_e}{\partial t^l} = \epsilon_0 \sum_{k=0}^{N_n} p_k \frac{\partial^k \mathbf{E}}{\partial t^k}, \quad (1)$$

where the reality of both \mathbf{P}_e and \mathbf{E} requires p_k 's and q_l 's to be real numbers. Keeping causal solutions for \mathbf{P}_e , it remains to carry out a Fourier transform with the following convention $\hat{f}(\omega) = \int_{\mathbb{R}} f(t) e^{-i\omega t} dt$:

$$\left(\sum_{l=0}^{N_d} q_l (i\omega)^l \right) \hat{\mathbf{P}}_e = \epsilon_0 \left(\sum_{k=0}^{N_n} p_k (i\omega)^k \right) \hat{\mathbf{E}}. \quad (2)$$

Then, the electric susceptibility $\hat{\chi}(\omega)$ is given by

$$\hat{\chi}(\omega) = \frac{\sum_{k=0}^{N_n} p_k (i\omega)^k}{\sum_{l=0}^{N_d} q_l (i\omega)^l}. \quad (3)$$

Using the fact that the electric susceptibility is expressed as a rational function, it is convenient to divide all the

coefficients by q_0 , and calling $P_k = p_k/q_0$, $Q_l = q_l/q_0$ equation (3) takes the form

$$\hat{\chi}(\omega) = \frac{\sum_{k=0}^{N_n} P_k (i\omega)^k}{\sum_{l=0}^{N_d} Q_l (i\omega)^l}, \quad Q_0 = 1. \quad (4)$$

Consider now, some experimental data determined for instance by ellipsometry given by a set of corresponding points $(\omega_m, \hat{\chi}_m^{Data})$ with $m = 0, \dots, M-1$. For passive materials these data are such that $\omega_m \in \mathbb{R}^+$ and $\hat{\chi}_m^{Data} \in \mathbb{C}^-$ were $\mathbb{C}^- = \{\xi \in \mathbb{C} | \text{Im}\{\xi\} < 0\}$. These data can be organized into the following vectors

$$\underline{\omega} = (\omega_0, \dots, \omega_{M-1})^T, \quad \underline{\hat{\chi}}^{Data} = (\hat{\chi}_0^{Data}, \dots, \hat{\chi}_{M-1}^{Data})^T. \quad (5)$$

Let's suppose that each $\hat{\chi}_m^{Data}$ at ω_m has a form as in Eq. (4), that is:

$$\hat{\chi}_m^{Data} = \frac{\sum_{k=0}^{N_n} P_k (i\omega_m)^k}{\sum_{l=0}^{N_d} Q_l (i\omega_m)^l}. \quad (6)$$

After some elementary manipulations and remembering that $Q_0 = 1$, Eq. (6) reads:

$$\hat{\chi}_m^{Data} = \sum_{n=0}^{N_n+N_d} r_n \xi_{m,n}, \quad (7)$$

with

$$r_n = \begin{cases} P_n & \text{if } n = 0, \dots, N_n \\ Q_{n-N_n} & \text{if } n = N_n + 1, \dots, N_n + N_d \end{cases}, \quad (8)$$

and

$$\xi_{m,n} = \begin{cases} (i\omega_m)^n & \text{if } n = 0, \dots, N_n \\ -\hat{\chi}_m^{Data} (i\omega_m)^{n-N_n} & \text{if } n = N_n + 1, \dots, N_n + N_d \end{cases} \quad (9)$$

This can be rewritten in matrix form as:

$$\underline{\hat{\chi}}^{Data} = \underline{\Xi} \underline{r}, \quad (10)$$

where \underline{r} is the column vector with entries r_n , with $n = 0, \dots, N_n + N_d$ and $\underline{\Xi}$ is the $M \times (N_n + N_d + 1)$ matrix with entries $\xi_{m,n}$. This overdetermined system can be solved in the sense of least squares [9]. That is, to find the vector \underline{R} such that

$$\|\underline{\Xi} \underline{R} - \underline{\hat{\chi}}^{Data}\|_2 = \min_{\underline{r} \in \mathbf{R}^{N_n+N_d+1}} \|\underline{\Xi} \underline{r} - \underline{\hat{\chi}}^{Data}\|_2. \quad (11)$$

This can be achieved, for instance, by the Householder transformation method [10]. In practice, we consider the

entries of \underline{r} to be complex, which relaxes our numerical scheme involving complex polynomials in $(i\omega)$. The imaginary part of these numbers remains several orders of magnitude smaller than their real part.

Once the p_k 's and q_l 's coefficients have been determined, it is possible to obtain the poles and zeros of $\hat{\chi}(\omega)$ by finding the roots of $\sum_{k=0}^{N_n} P_k (i\omega)^k$ and $\sum_{l=0}^{N_d} Q_l (i\omega)^l$ respectively. Let Ω_j , $j = 1, \dots, N_d$ be the obtained poles then $\hat{\chi}(\omega)$ can be expanded as follows [11]:

$$\hat{\chi}(\omega) = \sum_{j=1}^{N_d} \frac{A_j}{\omega - \Omega_j} + g(\omega), \quad (12)$$

where g is an holomorphic function representing a non resonant term of $\hat{\chi}$ and is approximated by a polynomial of degree $N_n - N_d$. Assuming that this non resonant term is negligible, the amplitude coefficients A_j 's can be obtained via the Tetrachotomy method [12] or as in the case of this paper by another least squares procedure. Note that this latest assumption simply amounts to compelling the degree of the numerator to be smaller than the denominator's.

3 Fitting data in practice

The first important step for fitting the data is to extend $\underline{\omega}$ and $\underline{\hat{\chi}}^{Data}$, which are always given for positive frequencies only, so that the new vectors represent an electrical susceptibility with Hermitian symmetry. Second, we set $N_d = 2J$ for $J \in \mathbb{N}$ and $N_n \leq N_d$. This is done keeping in mind that each pole Ω_j have its corresponding symmetric $-\Omega_j$ and in order to ensure that the non resonant function g is at most a constant. In practice a good choice is to keep $N_n = N_d$, which is the approach we will follow in the sequel. Next, when the poles Ω_j and the associated amplitudes A_j are computed, it is handy to sort these pairs by the modulus of A_j . Once the data sorted, the sign of the imaginary part of ω_j has to be checked. In the case of our choice for the Fourier Transform, the imaginary part of physical poles ω_j must be non negative. If the first J_p pairs of poles $(\Omega_j, -\overline{\Omega_j})$, with $J_p \leq J$, have non negative imaginary part, then we can truncate the limit of the sum in Eq. (12), that is:

$$\hat{\chi}_{trunc}(\omega) \approx \sum_{j=1}^{J_p} \frac{A_j}{\omega - \Omega_j} - \frac{\overline{A_j}}{\omega + \overline{\Omega_j}}. \quad (13)$$

It is easy to see that this expression presents Hermitian symmetry. Finally, if the error between $\hat{\chi}_{trunc}(\underline{\omega})$ and

$\hat{\chi}^{Data}$ according to a given norm is less than a certain tolerance, one can say the best fitting, according to this procedure, has been found. Otherwise it is necessary to repeat this procedure with $J+1$ points of poles and so on. It can be thought at first that the bigger the number of poles J the better will be the fitting. This is not true in general. As an illustrative example, the two and infinity norms fitting errors for Si [13] are shown in Figures 1 and 2 respectively. Notice that while the norm two error decreases as J increases, the norm infinity error does not exhibit a monotonic behavior. This is mainly due to the fact that the experimental data can exhibit measurement artefacts, for instance when switching from one source to another, and these small artefacts are revealed by the presence of spurious poles sometimes lying in the wrong (lower) half of the complex plane. These sharp spikes make the infinity norm increase once obvious poles are found.

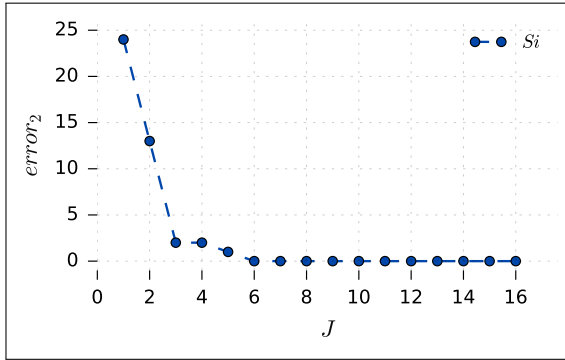


Figure 1: Norm two fitting error for Silicon as a function of the number of poles J

4 Results

The following tables are present the values of the poles ω_j and associated amplitudes $A_j = |A_j| \exp(i\phi_j)$ found when applying the method described above for different data sets. Also, the errors for 2-norm and ∞ -norm expressed in percentage are given. The materials considered in this paper are: Gold and Copper [14], Aluminum [15], Silver [16], GaAs, GaP [17] and Silicon [13]. The values for Au and Cu can be read in Tables 1 and 2, for wavelengths λ in the range $\lambda : 0.188 - 1.937\mu m$. In the same way, Tables 3 and 4 show the fitting values for Al and Ag with $\lambda : 0.667 - 200\mu m$ and $\lambda : 0.2066 - 12.40\mu m$ respectively.

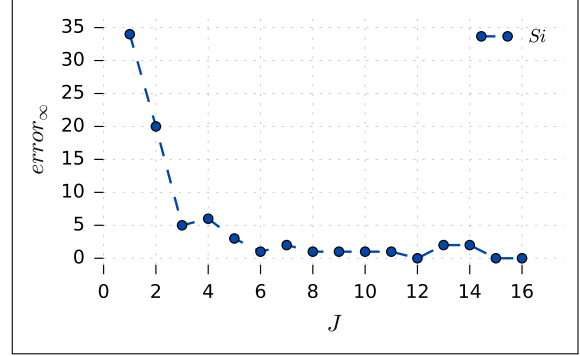


Figure 2: Norm infinity fitting error for Silicon as a function of the number of poles J

Finally, for the case of semiconductors, GaAs and GaP parameters are given in Table 5 and 6 for $\lambda : 0.234 - 0.840\mu m$ while Si parameters are written in Table 7 for $\lambda : 0.25 - 1.0\mu m$. These values were computed using the Python Code provided in (Ref. [18]).

Table 1: **Au (Johnson and Christy)**
 $\lambda : 0.188 - 1.937\mu m$

Ω_j [P rad/s]	$ A_j $	ϕ_j [rad]
$3.43E - 01 + 5.21E - 02i$	238.36	-3.14
$4.56E + 00 + 1.46E + 00i$	9.83	-2.12
error ₂ (%)	3.01	
error _∞ (%)	1.27	

Table 2: **Cu (Johnson and Christy)**
 $\lambda : 0.188 - 1.937\mu m$

Ω_j [P rad/s]	$ A_j $	ϕ_j [rad]
$4.46E - 01 + 4.61E - 02i$	156.78	-3.12
$3.11E + 00 + 7.71E - 01i$	5.16	-1.07
error ₂ (%)	6.70	
error _∞ (%)	2.88	

5 Validation

In order to test the validity of our approach, two comparisons have been realized between our results and the ones found in the literature. In the case of metals, the results reported by Barchiesi and Grosjes (B&G) in [7] for Gold

Table 3: **Al (Ordal et al.)** $\lambda : 0.667 - 200\mu\text{m}$

Ω_j [P rad/s]	$ A_j $	ϕ_j [rad]
$3.24E - 10 + 1.35E - 03i$	4284.43	-1.57
$1.13E - 01 + 7.16E - 02i$	228.84	-3.08
$4.24E - 01 + 7.94E - 01i$	139.21	0.69
$error_2$ (%)	8.36	
$error_\infty$ (%)	11.55	

 Table 4: **Ag (Babar et al)** $\lambda : 0.2066 - 12.40\mu\text{m}$

Ω_j [P rad/s]	$ A_j $	ϕ_j [rad]
$-9.14E - 16 + 6.52E - 02i$	1818.56	1.57
$8.37E + 00 + 2.78E + 00i$	6.83	-2.44
$6.30E + 00 + 4.72E - 01i$	1.62	-2.58
$6.73E + 00 + 2.18E - 01i$	0.39	-1.55
$error_2$ (%)	1.71	
$error_\infty$ (%)	1.87	

 Table 5: **GaAs (Jellison et al.)** $\lambda : 0.234 - 0.840\mu\text{m}$

Ω_j [P rad/s]	$ A_j $	ϕ_j [rad]
$7.17E + 00 + 8.55E - 01i$	18.54	-2.92
$4.65E + 00 + 1.00E + 00i$	12.34	-2.96
$4.30E + 00 + 2.57E - 01i$	2.37	-1.54
$7.66E + 00 + 2.40E - 01i$	1.79	1.29
$error_2$ (%)	3.13	
$error_\infty$ (%)	6.23	

 Table 6: **GaP (Jellison et al.)** $\lambda : 0.234 - 0.840\mu\text{m}$

Ω_j [P rad/s]	$ A_j $	ϕ_j [rad]
$7.60E + 00 + 7.60E - 01i$	20.56	-3.10
$5.64E + 00 + 2.40E - 01i$	5.02	-2.87
$6.19E + 00 + 3.51E - 01i$	1.96	-2.62
$4.32E + 00 + 4.49E - 01i$	0.68	-1.87
$error_2$ (%)	3.16	
$error_\infty$ (%)	6.78	

 Table 7: **Si (Green and Keevers)** $\lambda : 0.25 - 1.0\mu\text{m}$

Ω_j [P rad/s]	$ A_j $	ϕ_j [rad]
$7.99E + 00 + 1.83E + 00i$	13.57	2.98
$6.54E + 00 + 3.74E - 01i$	11.50	2.78
$5.49E + 00 + 6.65E - 01i$	10.51	-2.46
$5.12E + 00 + 1.68E - 01i$	4.02	-2.46
$error_2$ (%)	1.08	
$error_\infty$ (%)	3.08	

(using experimental data from [14]). In this case we set $J = 8$ and truncate the sum up to $J_p = 2$ (the same number of poles considered by B&G). The errors using 2-norm and ∞ -norm expressed in percentage obtained by us are 3.01% and 1.27%, while for B&G are 9.98% and 6.65% respectively. For semiconductors, the Deinega and John (D&J) fitting parameters obtained for Silicon by considering two poles allow to compute a 2-norm error of 8.5% and a ∞ -norm error of 15.63%. On the other hand, our approach setting $J = 6$ and $J_p = 4$ (the double of poles than D&J) allow us to compute corresponding two and infinity norm errors of 1.08% and 3.08%.

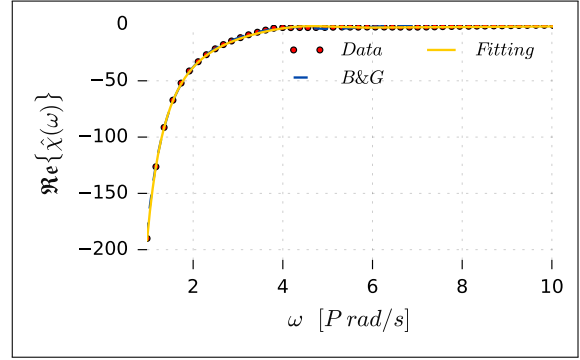


Figure 3: Comparison between the experimental data, the approach by Barchiesi and Grosgees (B&G) and our fitting for the real part of $\hat{\chi}$ for Gold.

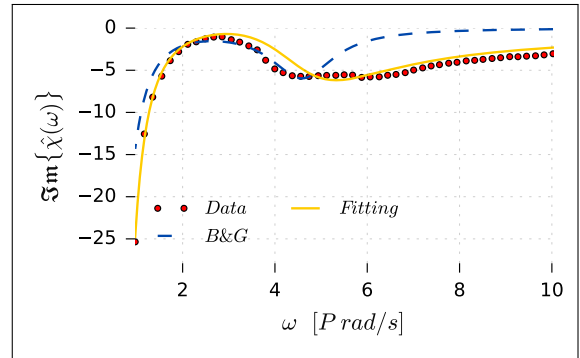


Figure 4: Comparison between the experimental data, the approach by Barchiesi and Grosgees (B&G) and our fitting for the imaginary part of $\hat{\chi}$ for Gold.

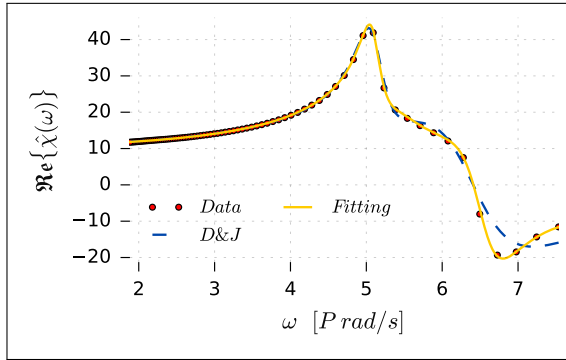


Figure 5: Comparison between the experimental data, the approach by Daneiga and John (D&J) and our fitting for the real part of $\hat{\chi}$ for Silicon.

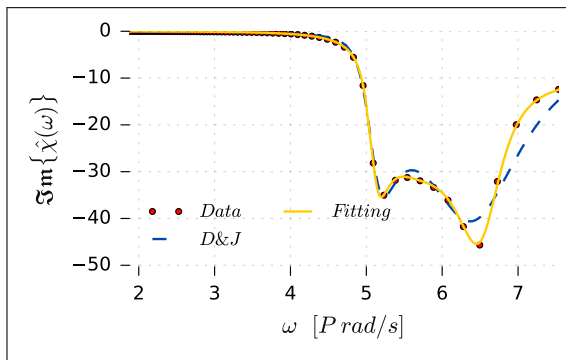


Figure 6: Comparison between the experimental data, the approach by Daneiga and John (D&J) and our fitting for the imaginary part of $\hat{\chi}$ for Silicon.

6 Conclusions

In this letter, we proposed a simple yet systematic procedure for fitting experimental data of permittivities of resonant materials such as metals and semiconductors in the visible range. This procedure does not assume *a priori* any particular shape for the electric susceptibility $\hat{\chi}$. The final expression obtained for the permittivity preserves causality and stability. This fitting is more accurate than those presented in the reviewed literature. It can be used as it is in numerical codes such as FDTD.

References

- [1] E. D. Palik, *Handbook of optical constants of solids*, vol. 3. Academic press, 1998.
- [2] M. J. Weber, *Handbook of optical materials*, vol. 19. CRC press, 2002.
- [3] A. Taflove and S. C. Hagness, *Computational electrodynamics*. Artech house publishers, 2000.
- [4] T. Lu, P. Zhang, and W. Cai, “Discontinuous galerkin methods for dispersive and lossy maxwell’s equations and pml boundary conditions,” *Journal of Computational Physics*, vol. 200, no. 2, pp. 549–580, 2004.
- [5] Y. Brûlé, B. Gralak, and G. Demésy, “Calculation and analysis of the complex band structure of dispersive and dissipative two-dimensional photonic crystals,” *JOSA B*, vol. 33, no. 4, pp. 691–702, 2016.
- [6] P. G. Etchegoin, E. Le Ru, and M. Meyer, “An analytic model for the optical properties of gold,” *The Journal of chemical physics*, vol. 125, no. 16, p. 164705, 2006.
- [7] D. Barchiesi and T. Grosjes, “Errata: Fitting the optical constants of gold, silver, chromium, titanium and aluminum in the visible bandwidth,” *Journal of Nanophotonics*, vol. 8, no. 1, p. 089996, 2015.
- [8] A. Deinega and S. John, “Effective optical response of silicon to sunlight in the finite-difference time-domain method,” *Optics Letters*, vol. 37, pp. 112–114, Jan. 2012.
- [9] G. Strang, *Linear Algebra and Its Applications*. Thomson, Brooks/Cole, 2006. Google-Books-ID: 8QVdcRjyL2oC.

-
- [10] Y. Skiba, *Metodos Y Esquemas Numericos : Un Analisis Computacional*. UNAM, June 2005.
- [11] R. Petit, *L'outil mathématique: distributions, convolution, transformations de Fourier et de Laplace, fonctions d'une variable complexe, fonctions eulériennes*. Masson, 1991.
- [12] F. Zolla, *Foundations of Photonic Crystal Fibres*. Imperial College Press, Jan. 2005. Google-Books-ID: iVZXwXDswv0C.
- [13] M. A. Green and M. J. Keevers, "Optical properties of intrinsic silicon at 300 K," *Progress in Photo-voltaics: Research and Applications*, vol. 3, pp. 189–192, Jan. 1995.
- [14] P. B. Johnson and R. W. Christy, "Optical Constants of the Noble Metals," *Physical Review B*, vol. 6, pp. 4370–4379, Dec. 1972.
- [15] M. A. Ordal, R. J. Bell, R. W. Alexander, L. A. Newquist, and M. R. Querry, "Optical properties of Al, Fe, Ti, Ta, W, and Mo at submillimeter wavelengths," *Applied Optics*, vol. 27, pp. 1203–1209, Mar. 1988.
- [16] S. Babar and J. H. Weaver, "Optical constants of Cu, Ag, and Au revisited," *Applied Optics*, vol. 54, pp. 477–481, Jan. 2015.
- [17] G. E. Jellison, "Optical functions of silicon determined by two-channel polarization modulation ellipsometry," *Optical Materials*, vol. 1, pp. 41–47, Jan. 1992.
- [18] M. Garcia-Vergara, G. Demésy, and F. Zolla, "Hunting complex poles," (GitHub 2016) [retrieved 6 Dec 2016]. <https://git.io/v14Jb>.